Contribution of photic and aphotic N₂ fixation to production in an oligotrophic sea

Etai Landou [ORCID],[1]* Boaz Lazar [ORCID],[2] Julie LaRoche [ORCID],[3] Katja Fennel [ORCID],[4] Ilana Berman-Frank [ORCID][5]*
[1]Mina and Everard Goodman Faculty of Life Sciences, Bar-Ilan University, Ramat Gan, Israel
[2]Fredy and Nadine Herrmann Institute of Earth Sciences, Hebrew University of Jerusalem, Jerusalem, Israel
[3]Department of Biology, Dalhousie University, Halifax, Nova Scotia, Canada
[4]Department of Oceanography, Dalhousie University, Halifax, Nova Scotia, Canada
[5]Department of Marine Biology, Leon H. Charney School of Marine Sciences, University of Haifa, Haifa, Israel

Abstract

Dinitrogen (N₂) fixation was investigated at a pelagic station in the oligotrophic waters of the northern Gulf of Aqaba, Red Sea, between February 2016 and December 2018. In situ $^{15}N_2$ and ^{13}C incubations were used to evaluate photic and aphotic N₂ fixation rates and diazotrophic contribution to water column productivity. N₂ fixation rates were typically low (below detection to <0.5 nmol N L^{-1} d^{-1}). Maximal rates of 3.1 nmol L^{-1} d^{-1}, measured at 100 m when conspicuous slicks of the cyanobacterium *Trichodesmium* appeared on the surface water. Amplicon sequencing of *nifH* demonstrated that non-cyanobacterial diazotrophs, mostly α- and γ-proteobacteria comprised the majority (82–100%) of amplicon sequence variants retrieved from photic and aphotic depths when low N₂ fixation rates were measured, while amplicons representing cyanobacteria were nearly absent, but appeared in low abundance (∼ 2%) when maximal rates were measured. During the stratified summer-period, water-column N₂ fixation rates (10–75 μmol m^{-2} d^{-1}) comprised ∼ 1–40% of new production (NP). During the winter mixing period N₂ fixation rates were considerably higher (11–242 μmol m^{-2} d^{-1}) but made up only <1% of NP. This is because, during this period, nitrate supplied to the photic zone by the vertical mixing becomes the major N source for NP. We conclude that on an annual average, diazotrophy plays a minor role in the NP of the Gulf. The major "new" nitrogen sources are cross-thermocline turbulent diffusion of nitrate during summer stratification and vertical mixing during the fall–winter.

Constraining the contribution of different nitrogen sources to new and export production for reliable reconstructions of oceanic nitrogen budgets remains a challenge. Biological N₂ fixation is an important source of nitrogen supporting new production (NP) (i.e., the fraction of primary production supported by nitrogen sources external to the photic zone) (Dugdale and Goering 1967; Capone and Carpenter 1982). The reports of N₂ fixation contributions to NP vary from ∼ 0% to 90% depending on location, season, and the specific diazotroph (dinitrogen fixers) populations (Capone et al. 2005; Moreira-Coello et al. 2017; Caffin et al. 2018). N₂ fixation also occurs in the aphotic (deep and dark) water column, likely driven by non-cyanobacterial diazotrophs (NCD) (Bonnet et al. 2013; Rahav et al. 2013; Benavides et al. 2015), although cyanobacteria transported to these depths may also retain some temporary capacity for nitrogen fixation (Benavides et al. 2022). Aphotic N₂ fixation can impact the global estimate of N₂ fixation due to the extensive volume of the aphotic ocean (Benavides et al. 2018; Zehr and Capone 2020). The high degree of uncertainty in both the distribution of diazotrophs and reported rates of N₂ fixation (Tang et al. 2019; White et al. 2020) has motivated expanding N₂ fixation studies beyond the traditionally surveyed sunlit waters of the tropical and subtropical ocean gyres (Mulholland et al. 2012; Harding et al. 2018; Shiozaki et al. 2020).

The Gulf of Eilat/Aqaba (herewith, the Gulf) is a semi-enclosed basin located at the northern tip of the Red Sea (Fig. 1). The oligotrophic water column of the Gulf is characterized by a well-defined annual cycle of mixing and stratification

*Correspondence: landoue@biu.ac.il; iberman2@univ.haifa.ac.il

Additional Supporting Information may be found in the online version of this article.
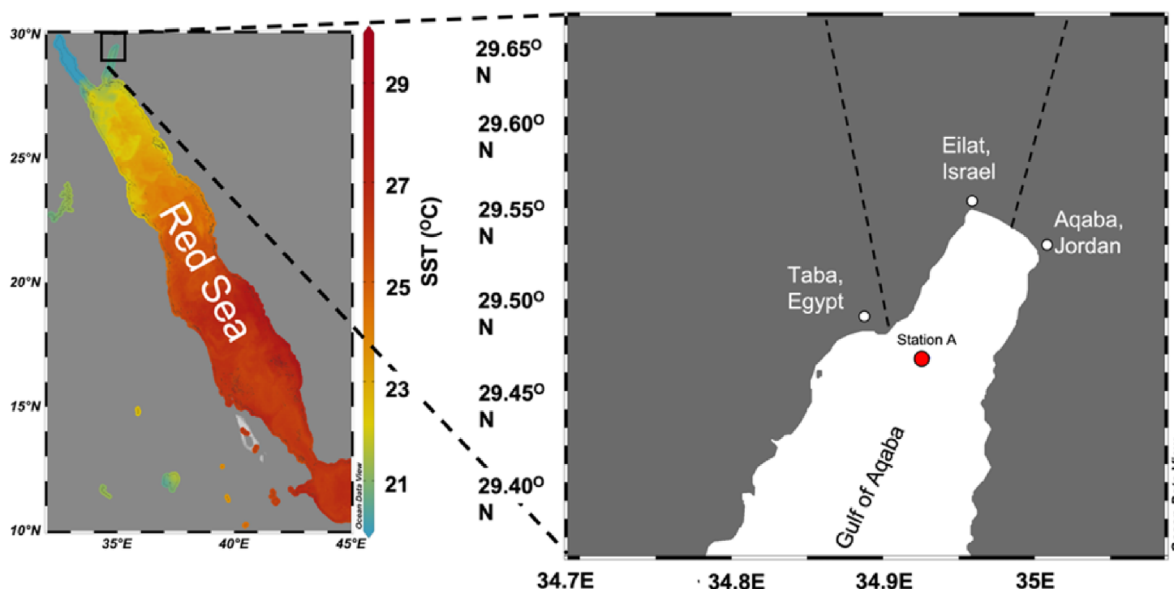
Fig. 1. Study site at the northern Gulf of Eilat/Aqaba (the Gulf), Red Sea (*see* inset), showing St. A (red dot, location 29°28′N, 34°55′ E, bottom depth ∼ 720 m). The water column characteristics of St. A are representative of the oligotrophic open waters of the Gulf.

(Levanon-Spanier et al. 1979; Wolf-Vecht et al. 1992) and primary productivity (PP) ranging from ∼ 100–170 g C m^{-2} yr^{-1} (Levanon-Spanier et al. 1979; Shaked and Genin 2021). Water column density stratification in the Gulf (and the Red Sea) is rather weak because the temperature of the deep-water column below the thermocline is very high (∼ 20°C). Hence, the depth of the mixed layer during winter vertical mixing is determined by the heat loss across the air–sea interface (Biton and Gildor 2011; Carlson et al. 2014). During particularly cold winters this can cause mixing down to > 700 m (Genin et al. 1995; Lazar et al. 2008). The supply of nutrients into the photic zone by vertical mixing results in mesotrophic conditions (NO$_3^-$ can reach up to ∼ 2000 nmol L^{-1} and PO$_4^{3-}$ > 100 nmol L^{-1}) and PP of 0.3–0.7 g C m^{-2} d^{-1} (Meeder 2012; Shaked and Genin 2021). At the onset of thermal stratification in spring, a sharp shoaling of the mixed layer occurs, which traps substantial amounts of nutrients in the photic zone and triggers a phytoplankton "spring-bloom" at the surface water (Genin et al. 1995; Lazar et al. 2008). The spring phytoplankton blooms utilize most of the nutrients in the photic zone and subsequently the upper ∼ 100 m water column may become oligotrophic (Lindell and Post 1995; Mackey et al. 2009).

Nitrogen is considered a limiting nutrient to primary producers in the Gulf from the onset of stratification to the beginning of mixing (Levanon-Spanier et al. 1979; Al-Qutob et al. 2002; Suggett et al. 2009). The water column inventory of dissolved inorganic nitrogen (DIN = NO$_3^-$ + NO$_2^-$), integrated over the whole water column, reaches ∼ 2.5 mol N m^{-2} during summer stratification and decreases by ∼ 50% during winter mixing due to the higher phytoplankton productivity during this period (according to data collected regularly by the

National Monitoring Program [NMP] since 2003; Fig. 2). Dissolved organic nitrogen was estimated from discrete measurements across the water column at ∼ 3.5 mol N m^{-2} with observed seasonal variations of 0.4 mol N m^{-2} between summer and winter (Meeder 2012). Exported particulate organic nitrogen (PON) was assessed from bulk particulate fluxes at ∼ 0.5 mol N m^{-2} yr^{-1} (Torfstein et al. 2020).
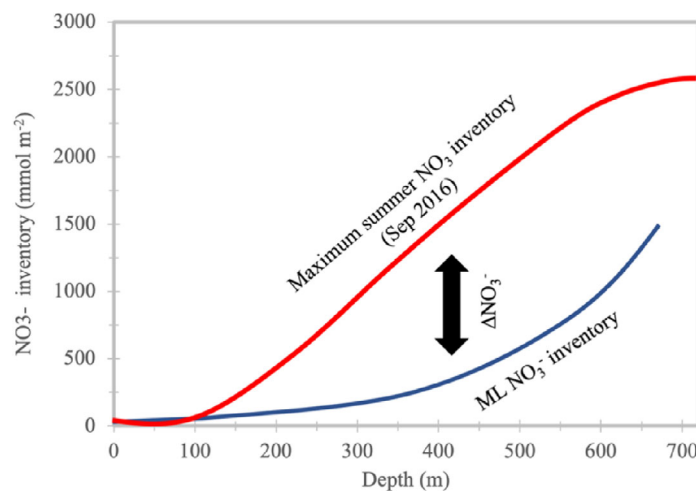
Fig. 2. Calculation of the assimilated NO$_3^-$ (ΔNO$_3^-$) for the mixing period 2016–2017 to estimate NP. The lines represent the best fit for the curves representing (1) the NO$_3^-$ inventory during the maximal water column inventory of NO$_3^-$ (September 2016; red line) and (2) the curve representing the NO$_3^-$ inventories in the ML as constructed from the NO$_3^-$ depth profiles of every cruise during the winter mixing of 2016–2017 (between October 2016 and February 2017; blue line).

The role of N_2 fixation as a nitrogen source in the Gulf is not well constrained. Surveys of *nifH* genes in the northern Gulf identified diverse diazotroph communities, including cyanobacteria, α- and γ-proteobacteria, and several uncultured phylotypes (Foster et al. 2009). The conspicuous filamentous cyanobacterial diazotroph, *Trichodesmium*, is found regularly in low abundance at depths ranging from surface and down to 100 m (Kimor and Golandsky 1977; Post et al. 2002; Rahav et al. 2013) and stochastically forms observable surface slicks (Gledhill et al. 2019; Wang et al. 2022). Yet, measurements of N_2 fixation rates in the open water of the northern Gulf are still sparse showing vertical (depth) and temporal variability. Only two published studies directly measured N_2 fixation rates in the Gulf using the $^{15}N_2$ assimilation technique (Foster et al. 2009; Rahav et al. 2013), while one study measured species-specific rates for concentrated *Trichodesmium* spp. colonies using the indirect acetylene reduction method (Post et al. 2002).

Reported N_2 fixation rates from $^{15}N_2$ measurements range from 0 to ~ 2 nmol N L^{-1} d^{-1} (Foster et al. 2009; Rahav et al. 2013). These studies utilized the $^{15}N_2$ gas bubble method to spike the seawater sample (Montoya et al. 1996), which may underestimate N_2 fixation (Mohr et al. 2010; Großkopf et al. 2012). Nevertheless, Rahav et al. (2013) reported significant N_2 fixation rates in the aphotic oxygenated water column of the Gulf and estimated that 35–77% of the total water column N_2 fixation rates occurred in the aphotic zone, down to 700 m (depth of measured station). To our knowledge, data depicting annual variations in the spatial and temporal water column N_2 fixation rates in the Gulf have not been published. Moreover, lack of simultaneous NP estimates (e.g., vertical transport of NO_3^-) from the previously published N_2 fixation studies in the Gulf hamper the attempt to estimate the overall contribution of N_2 fixation to the Gulf's NP.

In this study we (1) provide temporal information on N_2 fixation rates during an annual cycle in the photic and aphotic zones of a representative pelagic station (St. A) of the Gulf; (2) identify the main diazotrophic groups inhabiting the water column during the sampling period; and (3) determine the contribution of photic and aphotic N_2 fixation to primary and NP in the Gulf.

Materials and methods

Study site and sample collection

Eleven sampling cruises were conducted from February 2016 to December 2018 at St. A (29°28′N, 34°55′E), a ~ 700 m water column at the northern tip of the Gulf (Fig. 1). During each cruise, water samples were collected at seven discrete depths using a Seabird carousel (rosette) equipped with a CTD (Seabird 19 Plus) and sensors for temperature, salinity, photosynthetically active radiation (PAR quantum sensor, LiCOR LI-192SA) and chlorophyll *a* (Chl *a*) fluorescence (Turner designs,

Cyclops7). Unfiltered seawater samples for dissolved inorganic nitrogen ($NO_3^- + NO_2^-$; hereafter DIN) were collected in duplicates into 15 mL acid prewashed polyethylene plastic test tubes and kept refrigerated at 4°C in the dark until analysis was performed, no later than 3 d after collection. Seawater samples for ^{15}N and ^{13}C incubation experiments were collected into 4.6 L acid-cleaned polycarbonate bottles and divided as follows: (1) six bottles were sampled at each photic depth, three transparent ("light") bottles and three black colored ("dark") bottles (used to correct for dark carbon fixation by subtraction from the light bottles of the same depth); and (2) three bottles (only dark) were sampled at each aphotic depth. Seawater samples were collected from each depth into two (duplicate) 4.6 L bottles (each bottle was prewashed three times with the sampled seawater) for the analyses of POC and PON (concentrations and isotopic compositions) at the beginning of the incubation (time T_0). Triplicate 5 L seawater samples were collected into acid prewashed plastic containers (which were prewashed three times with the sampled seawater before collection) for DNA analyses. DNA samples were filtered immediately after collection on 0.2 μm Supor filter (PALL), transferred to liquid nitrogen, and stored at -80°C until analysis in the lab.

Chl *a* concentrations

Duplicate seawater samples were collected into 250 mL HDPC bottles and refrigerated at 4°C in the dark until filtration on 25 mm Whatman GF/F (ca. 0.7-μm pore size), no later than 4 h after collection. The filters were placed in 20 mL glass vials and extracted in 5 mL of 90% acetone overnight at 4°C in the dark. Blank filters were also stored in 90% acetone under the same conditions. Chl *a* concentration was measured fluorometrically using a Turner Designs. (TD-700) fluorometer with a 436 nm excitation filter and a 680 nm emission filter (Holm-Hansen et al. 1965). Calibration was performed with pure Chl *a* from *Anacystis nidulans* (Sigma-Aldrich C6144).

Inorganic nutrients

Concentrations of inorganic nutrients were determined by a flow injection autoanalyzer (Lachat Instruments Model QuikChem 8000). The analyses were calibrated with certified standard solutions of NO_3^-, NO_2^-, and PO_4^- (Merck). The limit of detection (LOD) was 0.05 and 0.03 μmol L^{-1} for DIN ($NO_3 + NO_2$) and PO_4^-, respectively.

$^{15}N_2$ Fixation and ^{13}C PP

The $^{15}N_2$ enriched seawater (ESW) was prepared using a modified $^{15}N_2$ ESW method (Mohr et al. 2010; Wilson et al. 2012). Filtered (0.2 μm) seawater were degassed using a degassing membrane (3M Liqui-Cel model G542) and transferred directly into 1.25 L Nalgene bottles fitted with a septum cap (filled to the top with no headspace) and 12.5 mL of pure $^{15}N_2$ gas (98% ^{15}N atoms, Cambridge Isotope Laboratories)

was injected into each bottle using a gas-tight syringe. After injection, the bottles were shaken vigorously for 10 min and stored at 4°C for 12–16 h to allow for equilibrium with the tracer. The atom% enrichment of each batch of $^{15}N_2$ ESW was determined no later than 1 week after the cruise by measuring the $^{14-14}N_2$ ($m/z = 28$), $^{14-15}N_2$ ($m/z = 29$), and $^{15-15}N_2$ ($m/z = 30$) on a membrane-inlet mass spectrometer (MIMS; Bay instruments). A ^{13}C stock solution was prepared by dissolving 1 g of $NaH^{13}CO_3$ (Sigma-Aldrich) in 100 mL of filtered (0.22 μm) double-distilled H_2O to a final concentration of 119 mmol L^{-1} $H^{13}CO_3^-$.

Seawater samples from each predetermined depth were filled into one 4.6 L incubation bottle and one 1 L bottle. A volume of 250 mL of seawater was removed from each incubation bottle and replaced by 230 mL of $^{15}N_2$ ESW stock solution and 1 mL of ^{13}C stock solution, leaving $\sim$ 20 mL of headspace. The bottle was then inverted three times and immediately topped with the sample water from the 1 L bottle (leaving no headspace). Incubations of the spiked samples were carried out immediately following tracer additions. Samples collected from photic depths were incubated in situ on a mooring line at the same depths from which the water had been collected. The mooring station was located $\sim$ 4 km northwest of St. A (29°30′N, 34°55′E; bottom depth 160 m). Aphotic samples were incubated onshore in the laboratory and maintained in dark containers filled with water that was kept at 21–22°C (the ambient water temperature in aphotic water). After 24 h, incubations were immediately terminated by filtering the entire contents of the bottles onto precombusted (at 450°C for 4 h) GF/F filters (25 mm Whatman GF/F, ca. 0.7 μm in pore size). Filters were stored at −20°C, dried (at 60°C overnight), pelletized in tin capsules and analyzed on a Variocube continuous-flow isotope ratio mass spectrometer (Elementar) at the Department of Oceanography, Dalhousie University (Halifax, NS, Canada).

N_2 fixation rates were calculated by a modified isotope mass balance equation (derivation available upon request) of Montoya et al. (1996) (Eq. 1):

$$N_2 \text{ fixation rate} = \frac{A_{PN_f} - A_{PN_0}}{A_{spike} \times (1 - f_{sw}) - A_{sw} \times f_{sw}} \times \frac{[PN]}{\Delta t} \quad (1)$$

where A_{PN} denotes the atom% of $^{15}N_2$ measured in the particulate organic N (PN) and the subscripts f and 0 denote the final and initial times of the incubation, respectively; A_{spike} and A_{SW} denote the $^{15}N_2$ atom% of the spiked seawater and the sample seawater, respectively. f_{sw} is the fraction of seawater in the mixture, where $f_{sw} + f_{spike} = 1$. [PN] is the concentration of particulate nitrogen measured on the filters at the end of the incubation and Δt is the incubation time ($t_f - t_0$). The final $^{15}N_2$ atom% in incubation bottles (2.67–2.99%) was calculated from the $^{15}N_2$ atom% of the ESW stock (the "spike"; 5% of the incubation volume) and $^{15}N_2$ atom% in the

incubation water (estimated from N_2 solubility of the sample water using solubility factors from Hamme and Emerson 2004). PP was calculated according to Mulholland and Bernhardt (2005).

Measurements of N_2 fixation rates and ^{13}C productivity were reported in this study only for samples with PN > 8 μg and POC > 9 μg. These values were calculated from the 3σ of the blanks for N and C samples, samples with lower values were defined as "below detection", and the values of these samples were taken as zero (Fig. S4). The values of $^{min}\Delta A_{POC}$ and $^{min}\Delta A_{PN}$ (minimum increment in the isotopic composition of POC and PN after the incubation with ^{13}C and ^{15}N spikes) were calculated as 3σ of the average isotopic values measured on natural (unspiked) particulate organic matter samples. The average $^{min}\Delta A_{PN}$ was 0.0011% and average $^{min}\Delta A_{POC}$ was 0.007%. To keep our N_2 fixations measurements conservative we calculated the LOD of N_2 fixation rates by setting $^{min}\Delta A_{PN}$ to 0.00146% (that is, 4‰ vs. air prescribed by Montoya et al. 1996), rather than our calculated value of 0.0011%. The $^{min}\Delta A_{POC}$ and $^{min}\Delta A_{PN}$ values (*see* above) were calculated together with specific POC and PON concentrations and incubation times (Table S2), resulting in an independent detection limit for each measurement (Gradoville et al. 2017; White et al. 2020). The calculated LOD for N_2 fixation ranged from 0.06 to 0.69 nmol N L^{-1} d^{-1}, and 0.08 to 0.22 μg C L^{-1} d^{-1} for carbon fixation. A sample was considered zero if two out of three replicates were below the LOD. The water column integrated parameters and their standard deviations were obtained by Gaussian Monte Carlo numerical integrations with 50,000 iterations. Samples forced to zero (*see* above) were also taken as zero when depth-integrated fluxes were calculated.

Estimation of NP and the *f* ratio

NP was defined as the sum of nitrogen fluxes from deep water (aphotic) NO_3^- (either by vertical mixing during winter or by cross-thermocline turbulent mixing and breaking internal waves during summer) and from N_2 fixation (Eq. 2):

$$F_{NP} = F_{aphotic\,NO_3^-} + F_{NF} \quad (2)$$

where F denotes N flux (mmol m^{-2} d^{-1}) and the subscripts NP, aphotic NO_3^- and NF denote new production, entrainment of deep water (aphotic) NO_3^-, and N_2 fixation, respectively.

Once NP is estimated, the contribution of N_2 fixation to NP can be assessed using Eq. 3:

$$NF = \frac{F_{NF}}{F_{NP}} \quad (3)$$

where NF is the fraction of N_2 fixation in NP.

Estimating NP during stratification

To estimate $F_{\text{aphotic NO}_3^-}$ during stratification the vertical diffusive fluxes of NO_3^- into the photic layer were calculated, following Fick's law from the product of the NO_3^- gradient through the thermocline. The NO_3^- gradient was obtained by linearly fitting nitrate concentrations within the thermocline at 120–200 m depth. $F_{\text{aphotic NO}_3^-}$ can then be estimated by Eq. 4:

$$F_{\text{aphotic NO}_3^-} = -Dx\frac{d\text{NO}_3}{dZ} \tag{4}$$

where $F_{\text{aphotic NO}_3^-}$ is the flux of aphotic NO_3 into the photic zone (mmol N m^{-2} d^{-1}), D is the overall (cross-thermocline turbulent mixing and breaking internal waves) turbulent diffusion coefficient (m^2 d^{-1}) and $\frac{d\text{NO}_3}{dZ}$ is the vertical gradient of NO_3^- (mmol N m^{-4}). The values of $\frac{d\text{NO}_3}{dZ}$ were estimated from the slope of best-fit line of NO_3^- measured within the thermocline at depths of 120–200 m. For the turbulent diffusion coefficient (D) we used 20 m^{-2} d^{-1}, a value calculated by David (2002) for St. A during stratification. NO_3^- fluxes for summer months (June–September) of 2016 and 2018 were used to estimate NP during stratification.

Estimating NP during mixing

During mixing practically all NO_3^- is supplied to the mixed layer by vertical mixing from the aphotic zone. This "new" NO_3^- is assimilated by the phytoplankton community and contributes to NP. The NP at this period was estimated following the method developed by Meeder (2012). The estimate is based on the difference between two curves constructed from the best fit of the NO_3^- depth profiles of cruises during the study period (Fig. 2) as follows: (1) the curve representing the maximal water column NO_3^- inventory for any depth interval between 0 m and z (in this study, we used the NO_3^- depth profile of September 2016, late summer just before the onset of mixing as represented by the red line in Fig. 2); and (2) the curve representing the NO_3^- inventories in the ML as constructed from the NO_3^- depth profiles of every cruise during winter mixing (in this study, we used the NO_3^- depth profiles of October 2016 to February 2017; blue line in Fig. 2). The difference between these two curves, here defined as ΔNO_3^-, provides a reliable estimate of NO_3^- assimilation by phytoplankton for any depth, when ML reaches a particular depth, $z_{\text{ML}} > z_{\text{photic zone}}$, where z_{ML} and $z_{\text{photic zone}}$ are the depths of the ML and photic zone, respectively. The $\Delta NO_3^-/\Delta t$ is the estimate of the NO_3^- assimilation rate, where Δt is the time elapsed between two consecutive ML depths (Δz_{ML}).

Estimating the *f* ratio during stratification

The fraction of NP from total primary production (new + regenerated) is referred to as the *f* ratio (Eppley and Peterson 1979). The *f* ratio during the stratified period was estimated by the equation:

$$f\ \text{ratio} = \frac{F_{\text{NP}}}{F_{\text{PP}}} \tag{5}$$

where *f* ratio is the fraction of new production from total primary production, F denotes N flux (mmol m^{-2} d^{-1}) and the subscripts NP and PP denote new production and primary production. F_{NP} was calculated as described in the sections above. F_{PP} was calculated using PP data obtained from ^{13}C incubations.

DNA extraction and *nifH* PCR analysis

DNA, from representative depths of the photic and aphotic layer, was extracted using a modified phenol–chloroform method described in Man-Aharonovich et al. (2007). For *nifH* gene amplification nested PCR was conducted using degenerate *nifH* primers. The nifH3 and nifH4 (Zani et al. 2000) primers were used for the first PCR. PCR reactions were performed using a Veriti thermocycler (Applied Biosystems). The first round of PCR contained 10X Platinum Taq PCR buffer (Thermo Fisher), MgCl (2.5 mmol L^{-1} final), dNTPs (0.2 mmol L^{-1} final), primers (1 μmol L^{-1} final), and 2 μL of DNA extract, adjusted to 25 μL total volume with nuclease free water. This reaction was cycled at 94°C for 5 min, 30 cycles of 94°C for 1 min, 57°C for 1 min, and 72°C for 1 min, and a final cycle of 72°C for 7 min. The second round of PCR used the same thermocycling conditions and components, but the DNA template was replaced with 1 μL of the PCR product from the first reaction and primers were replaced with nifH1 and nifH2 primers (Zehr and McReynolds 1989) attached to Illumina universal adaptors CS1 and CS2 and barcodes for demultiplexing in the Illumina MiSeq. No template controls (NTC) were included in each run. Samples were sequenced on Illumina MiSeq Standard v.3, 2 × 300 bp paired-end sequencing at Hy Laboratories Ltd.

Bioinformatic analyses

Raw data of demultiplex Illumina pair-end *nifH* DNA sequences were processed to amplicon sequence variants (ASVs) using DADA2 plugin (default setting) in QIIME2 (Bolyen et al. 2019). A total of 83,292 reads (28–50% of input reads; 6541–391 reads per sample) passed quality control. NTC were included in each sequencing run. Only one NTC sample contained sufficient DNA for sequencing. This sample contained 309 reads and 4 ASV which were compared with known contaminant sequences of PCR reagents or other sample processing procedures (Zehr et al. 2003). ASVs found in the NTC sample shared < 92% identity to known contaminates, and these ASVs were removed from downstream analysis. Following the removal of non-*nifH* sequences, and further evaluation of rarefaction curves, samples were normalized to 1316 sequences per sample (seq/sample) through a single rarefaction. Thus, only samples with sufficient reads to subsample down to 1316 sequences per sample were used ($n = 16$). To assign putative taxonomy, ASVs were annotated using BlastX against NCBI's non-redundant (NR) database, excluding

uncultured environmental sequences from search. Assignment to canonical clusters I-IV (Chien and Zinder 1996) was carried using the CART model (Frank et al. 2016). Trees was generated in MEGA 11 (Tamura et al. 2021) using the neighbor-joining method (Saitou and Nei 1987) with 1000 bootstrap replicates, and visualized using the Interactive Tree of Life (http://itol.embl.de). Raw sequences are available from NCBI Bioproject PRJNA880645.

Database information

The basic water column data we used in this study (e.g., temperature, Chl *a*, productivity) was collected during our cruises and supplemented by monthly data from the NMP in the Gulf. The NMP database is publicly available at:

https://iui-eilat.huji.ac.il/Research/NMPMeteoData.aspx.

Results

Ambient environmental conditions during the studied period

The annual dynamics of water column parameters between mixing and stratification periods during this study (2016–2018) reflect the typical annual pattern in the northern Gulf (NMP database for years 2003–2018; *see* methods). The maximum mixed layer depth (MLD) through the study period was 650 m observed during February 2017, reaching ~ 50 m above the bottom at St. A. The mixed layer potential temperature during the deep mixing of 2017 was uniform at $\sim 21.2°$C (Figs. 2a, S1). The maximal annual MLD was shallower in 2016 and 2018 (460 and ~ 300 m, respectively) (Figs. 2a, S1, S2; Table S1). The mixing period ends with a sharp shoaling of the MLD. During summers (June–October) a stable stratified layer (the seasonal thermocline) extended to a depth of ~ 200 m (deepening slowly during the summer) and surface water temperatures reached a maximum of $> 28°$C (Figs. 3, S1; Tables 1, S1). Surface water nutrients were low during summer stratification and substantially higher during winter mixing (Figs. 3b, S3). The nutrient depleted upper ~ 120 m layer (DIN $< 0.05\,\mu$g L^{-1}), which developed during summer stratification, resides within the thermocline and its bottom marks the thickness of the photic zone (Fig. 3b). Resulting surface nutrient concentrations during stratification correlated with the previous winter-mixing with higher surface nutrients measured following deep MLD (Figs. 3b, S3). During thermal stratification, DIN concentrations below the photic zone increased sharply at ~ 250 m (the nutricline) and then gradually increased from $\sim 2\,\mu$mol L^{-1} to a maximum of $\sim 6\,\mu$mol L^{-1} at 700 m (Figs. 3b, S3).

Chl *a* (an indirect proxy for photosynthetic biomass) corresponded to the maximum MLD during winter (Fig. 3c). During the summer stratification a deep chlorophyll maximum (DCM) with concentrations of 0.4–0.5 μg L^{-1} was observed at ~ 100 m (Fig. 3c; Table 1). During winter, the phytoplankton populations were mixed downward with the deepening MLD to depths substantially exceeding the depth of the photic zone.
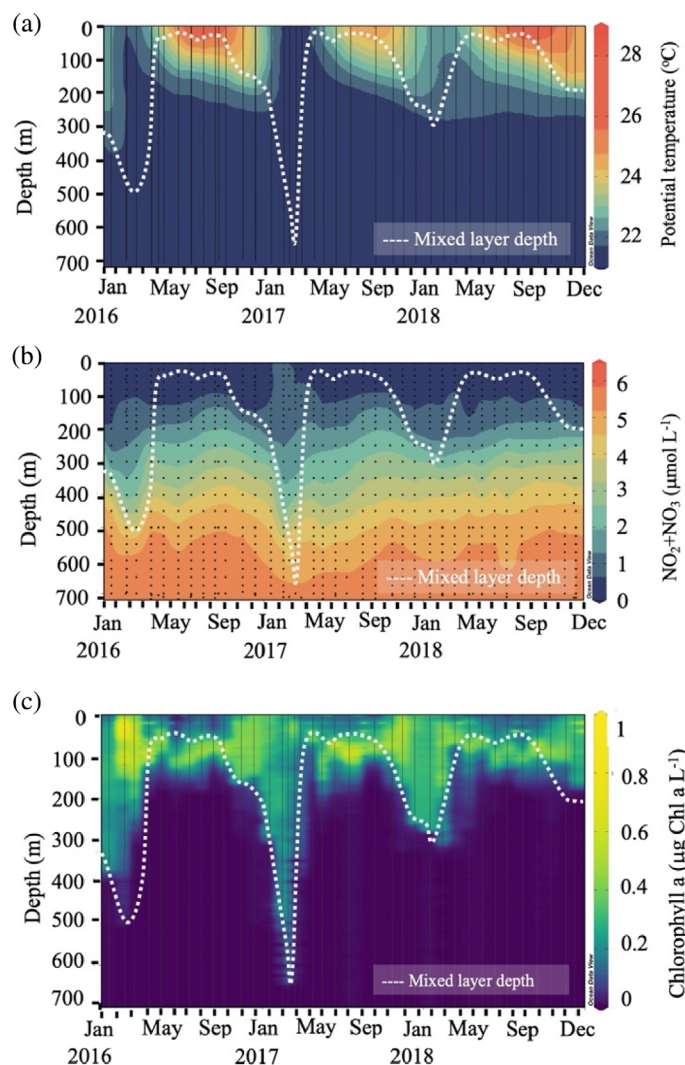
Fig. 3. Temporal dynamics of water column parameters at Sta. A (720 m bottom depth during the study period (2016–2018). (**a**) Potential temperature (colored contours); (**b**) DIN ($NO_3 + NO_2$, colored contours); and (**c**) Chlorophyll *a*. Data shown was collected during this study and monthly NMP cruises. The mixed layer depth (MLD) is represented by the white dashed lines. The contours and MLD were calculated from the continuous (CTD) and discrete (marked by the black dots) measurements.

This was demonstrated by the high and constant Chl *a* ($\sim 0.2\,\mu$g L^{-1}) concentration that reached down to ~ 550 m during the mixing season of 2017 (Fig. 3c). During the maximal annual mixing of 2016, 2017, and 2018 (MLDs of 480, 650, and 300 m, respectively), the integrated Chl *a* inventories were 190, 120, and 100 mg Chl *a* m^{-2}, respectively. During spring–summer transition periods, the Chl *a* inventory decreased markedly by a factor of 2–4 (40–50 mg m^{-2}). The DCM began developing at ~ 60 m during April–May (onset of stratification), deepened during stratification, and reached a maximum depth of 80–100 m during July–August. No DCM was observed when the mixing depth exceeded ~ 200 m (Fig. 3c).

Table 1. A summary of physical, chemical, and biological properties of the 700 m water column of St. A measured during 2016–2018. Ranges represent the minimum and maximum values measured under different hydrographic conditions (stratified water column, mixed water column, and transition-thermostabilizing period when the thermocline was stabilizing), in the photic and aphotic layers. The measured ranges of potential temperature (°C), salinity (PSU), dissolved inorganic nitrogen (DIN; μmol L^{-1}), Chl a (chlorophyll a; μg Chl a L^{-1}), PP (primary productivity; μg C L^{-1} d^{-1}), volumetric N$_2$ fixation rates (nmol N L^{-1} d^{-1}), and depth integrated N$_2$ fixation rates (μmol N m^{-2} d^{-1}) are shown. BLD—below detection limit.

Depths	Water column stability	Temp (°C)	Salinity	NO$_2$ + NO$_3$ (μmol L^{-1})	Chl a (μg Chl a L^{-1})	PP (μg C L^{-1} d^{-1})	N$_2$ fixation (nmol N L^{-1} d^{-1})	Integrated N$_2$ fixation (μmol N m^{-2} d^{-1})
Photic (0–120 m)	Mixing (Oct–Mar)	22–23	40.4–40.7	0.1–1.6	0.04–0.96	0.1–17	BLD–1.53	11–112
	Thermostablizing (Apr–May)	22–25	40.3–40.8	0.1–0.6	0.04–0.6	0.1–20	BLD–3.14	11–242
	Stratfied (Jun–Sep)	23–28	40.1–40.8	BLD–1	0.02–0.58	BLD–12	BLD–2.34	10–75
Aphotic (120–700 m)	Mixing (Oct–Mar)	21–23	40.4–40.6	0.2–5.9	BLD–0.37	BLD	BLD–1.05	44–265
	Thermostablizing (Apr–May)	21–23	40.4–40.8	0.1–6.1	BLD–0.21	BLD	BLD–1.71	45–645
	Stratfied (Jun–Sep)	21–23	40.5–40.8	0.6–6.1	BLD–0.29	BLD	BLD–0.22	21–42

Primary productivity

PP estimated from incubations with ^{13}C (in the same bottles as ^{15}N incubations) displayed typical water column profiles with the highest PP close to the surface, decreasing with depth, and reaching detection limits at depths of 120 m (Fig. 4a,b). The detectable volumetric PP rates varied 300-fold, ranging from 0.1 μg C L^{-1} d^{-1} in the deep photic zone (120 m) during December 2016, to 27 μg C L^{-1} d^{-1} in the surface water during April 2016. Maximum PP was measured during the spring transition period of March–April (corresponding to the phytoplankton "winter-spring blooms") (Fig. 4a,b). The range of the integrated PP varied by a factor of $\sim$ 4, ranging from 0.3 g C m^{-2} d^{-1} during the maximum stratification during July 2016 to 1.2 g C m^{-2} d^{-1} during the post mixing transition period in April 2016.

N$_2$ fixation rates

Volumetric and depth-integrated rates were calculated for two water layers, from surface to 120 m and from 120 to 700 m, corresponding to photic and aphotic layers, respectively. Volumetric rates in the photic zone ranged from below detection to 3.14 nmol N L^{-1} d^{-1} (May 2016; 100 m) (Fig. 4c,d). In the parallel dark incubations from photic depths, rates were typically similar or lower than ambient light incubation and ranged from below detection to 2.3 nmol N L^{-1} d^{-1} (May 2016; 100 m) (Fig. S6). Depth-integrated rates in the photic zone ranged from 11 μmol N m^{-2} d^{-1} (July 2018) to 242 μmol N m^{-2} d^{-1} (May 2016) (Fig. 5a).

Volumetric rates in aphotic water (120–700 m) ranged from below detection to 1.54 nmol N L^{-1} d^{-1} (May 2016; 300 m) (Fig. 4c,d). The depth-integrated rates in the aphotic zone ranged from 21 μmol N m^{-2} d^{-1} (July 2018) to 645 μmol N m^{-2} d^{-1} (May 2016) (Fig. 5a).

The relative contribution of photic and aphotic water layers to total N$_2$ fixation

The depth integrated N$_2$ fixation rates measured in aphotic depths accounted for 10–80% of total water column N$_2$ fixation (Fig. 5b). Aphotic N$_2$ fixation typically comprised > 50% of the total N$_2$ fixation during mixing while during the stratified and transition period it varied from 15% to 80% (Fig. 5b).

Diazotroph characterization

We assessed diazotrophic diversity by high-throughput sequencing of partial *nifH* gene sequences. A total of 116 ASVs were identified in our samples from different periods and depths. Phylogenetic analyses showed that amplified *nifH* gene sequences contained only a few cyanobacterial diazotrophs and mostly NCDs (Figs. 6, S7). Annotation of sequences using the CART model (Frank et al. 2016) suggested that sequences were from clusters I and III (Chien and Zinder 1996). Sequences were affiliated with Proteobacteria (α, γ, δ), Cyanobacteria, and Verrucomicrobia phyla.

NCDs comprised the majority of *nifH* sequences from both photic and aphotic depths with 82–100% of the amplicons annotated to NCDs from α- and γ-proteobacteria linage (Fig. S7). The predominant ASV in photic water was ASV89, closely related to the γ-proteobacteria *Pseudomonas stutzeri* (Fig. 6). This ASV was found in samples collected in July–September 2016 (stratified water; 5 m; 27–35% of the reads), February 2017 (deep mixing; 5 m; 16% of the reads) and April 2018 (transition from mixing to stratification; 100 m; 66% of the reads). Other abundant ASVs were ASV49, clustered with *Bradyrhizobium* spp. (α-proteabctria; Fig. 6) comprised 78% of the retrieved reads in the samples collected in photic depths during the transition from mixing to stratification (April 2016; 5 m). ASV104, clustered with *Azorhizobium* (α-proteabctria)
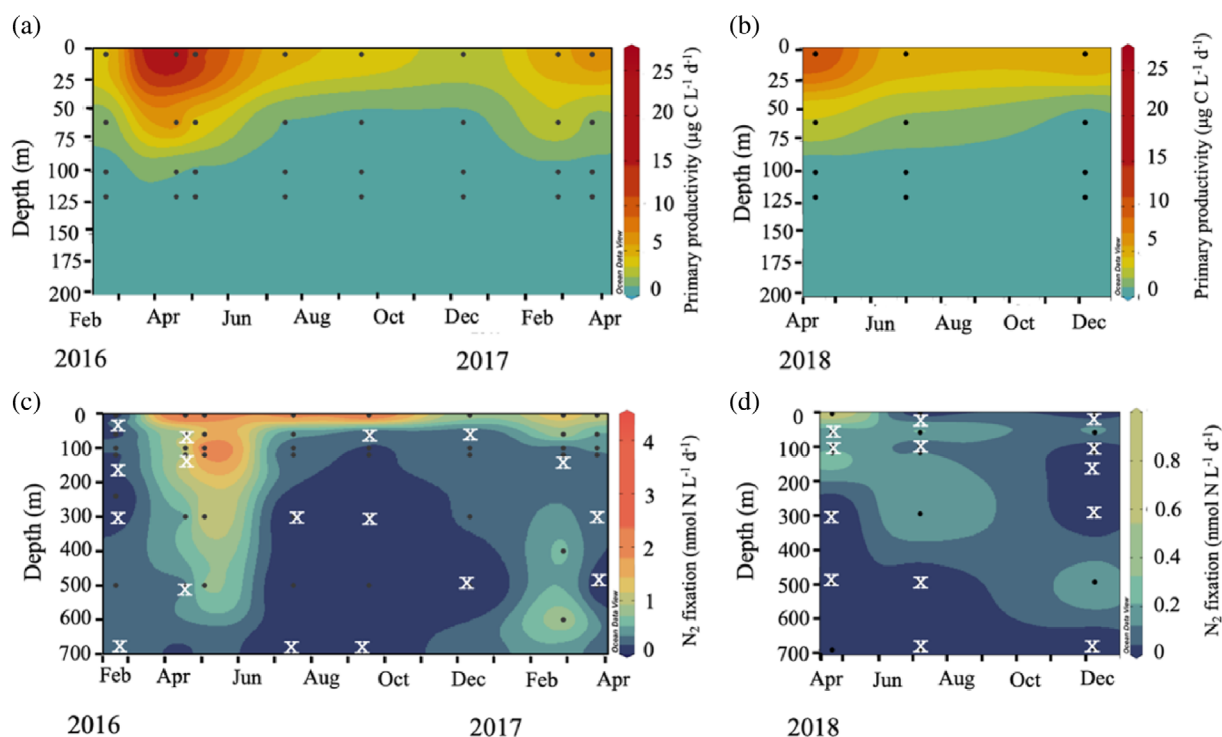
Fig. 4. Temporal dynamics of primary productivity (top panels; μg C L^{-1} d^{-1}), and N$_2$ fixation (bottom panels; nmol N L^{-1} d^{-1}) between February 2016–March 2017 (**a,c**) and April–December 2018 (**b,d**). Only the upper 200 m are shown for PP. Samples with N$_2$ fixation rates (**c,d**) below detection are marked by "x".
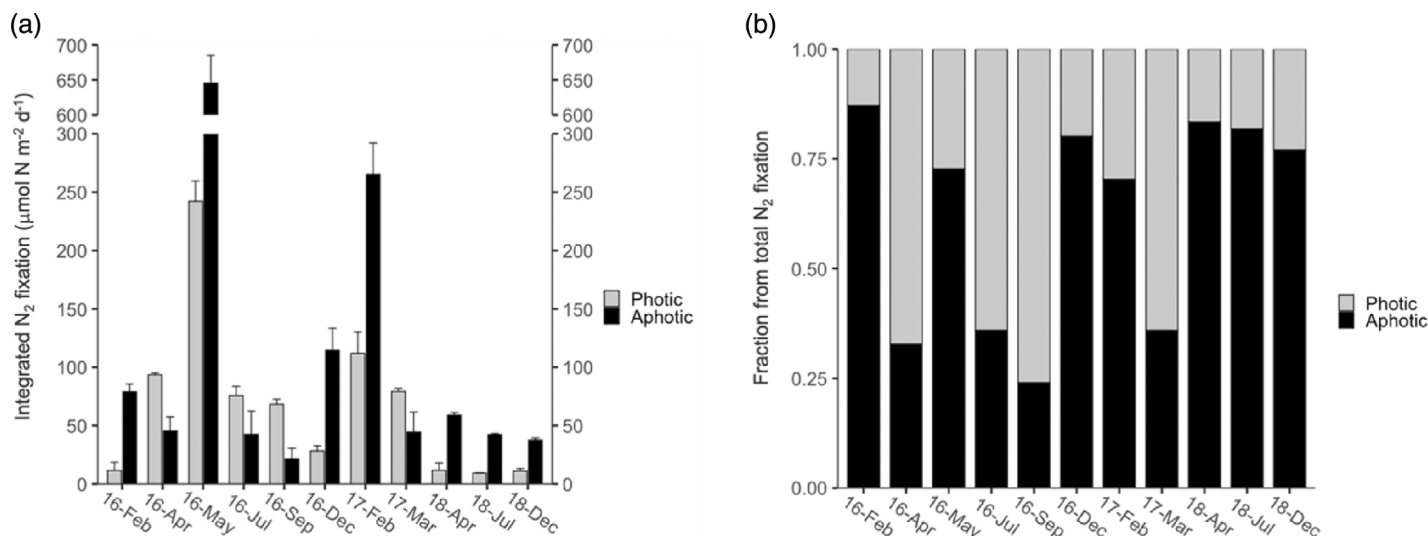
Fig. 5. Depth integrated rates of photic N$_2$ fixation (0–120 m, gray columns) and aphotic (120–700 m, black columns) within the 700 m water column of Sta. A in the Gulf. (**a**) Absolute depth-integrated values (μmol N m^{-2} d^{-1}); (**b**) relative contribution of aphotic and photic N$_2$ fixation from the total N$_2$ fixation. Results represent the average values of triplicates integrated using the trapezoid method.

comprised 81% of the reads during February 2017 (deep mixing; 5 m) but was absent from all other samples.

Aphotic waters samples were also characterized by predominance of ASV89 (Fig. S7) which comprised 45–95% of

the recovered amplicons during the transition period of 2016 (April 2016; 500 m and May 2016; 300 m) 24–87% of the reads during the stratified period of 2016 (July–September; 500 m;) and 95% of the retrieved sequences
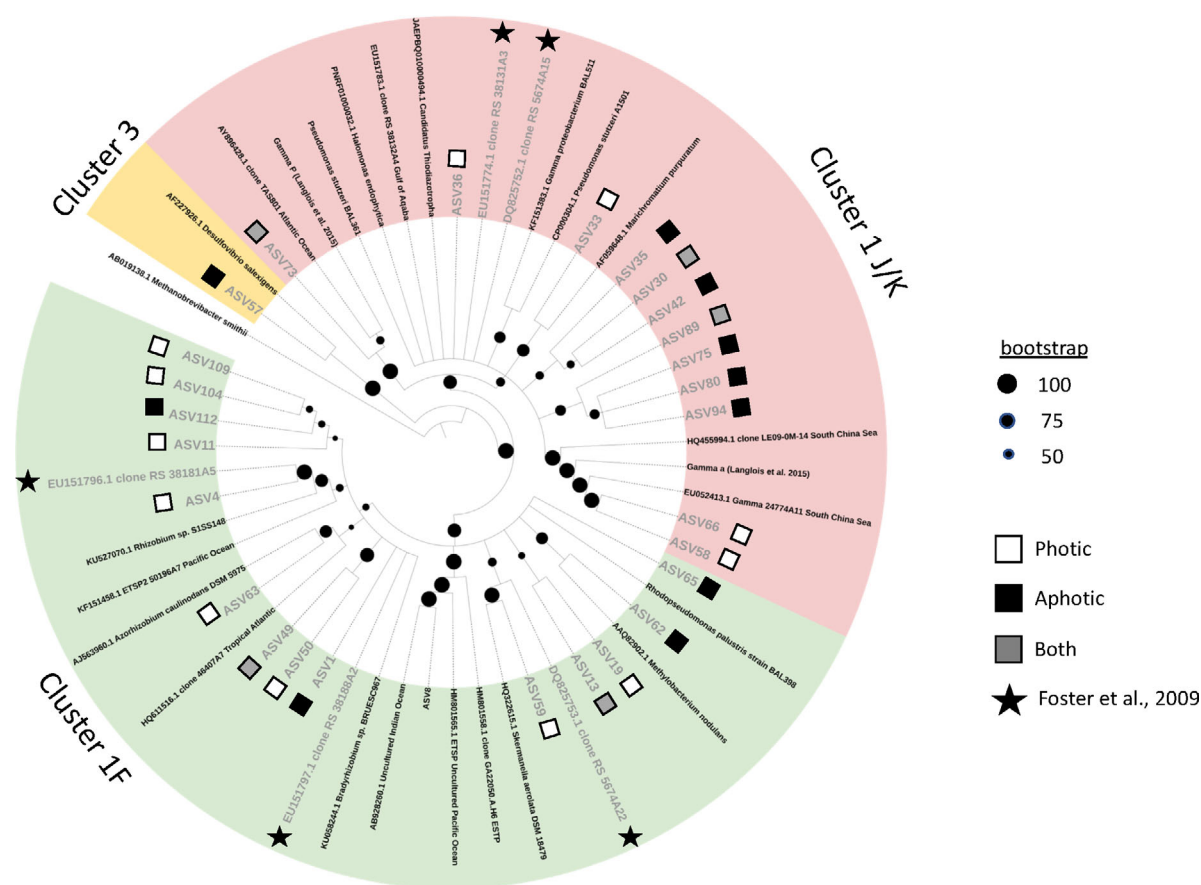
Fig. 6. Neighbor-joining phylogenetic tree derived from partial *nifH* amino acid sequences. The 15 most abundant ASVs retrieved from the photic layer (white squares) and aphotic layer (black squares) are shown. ASVs that appeared in samples collected from both photic and aphotic depths are marked by gray squares. These ASVs were used together with top hits from NCBI and (sequences with > 95% identity) to generate the tree. Sequences previously reported from the Gulf by Foster et al. (2009) that shared > 97% similarity to ASVs from this study are also shown (black stars). ASVs 66 and 58, clustered with the globally distributed NCD's Gamma-a (Langlois et al. 2015) and γ-24774A11 (Moisander et al. 2008) were included in the tree, although they were rarely recovered (2% of the reads in one sample). The tree was generated in MEGA 11 (Stecher et al. 2020) using the neighbor-joining method (Saitou and Nei 1987) with 1000 bootstrap replicates (Bootstrap values of > 50% marked on branches) and visualized using the Interactive Tree of Life (http://itol.embl.de/; Letunic and Bork 2021).

during the deep mixing (February 2017; 500 m). ASV35, also clustered with *Marichromatium purpuratum* and *P. stutzeri* (same clade as ASV89) comprised 88% of the reads during the transition from mixing to stratification (April 2018; 300 m). ASV13, closely related to *Methylobacterium nodulans* (*a*-proteobacteria) comprised 57% of the sequences recovered in September 2016 (500 m). ASV65, affiliated with *Rhodopseudomonas palustris* (*a*-proteobacteria) comprised 40% of the reads in samples from April 2016 (500 m) (Figs. 6, S7).

ASVs 58 and 66 clustered with the widely distributed NCD Gamma-A (Fig. 6). Yet, these sequences were recovered from one sample (September 2016; 5 m) and comprised only 2% of the retrieved reads.

Amplicons affiliated with cyanobacterial phylotypes (ASVs 51–53) were found only in two samples: May 2016 (100 m) and February 2017 (5 m). These ASVs comprised < 2% of the

total retrieved amplicons and clustered with *Microcoleaceae* (ASV51) and UCYN-A (ASV52-53) (Fig. S8).

Estimating NP during mixing

Turbulent diffusion during winter is negligible compared to NO_3^- introduced by vertical mixing (Meeder 2012). we used NO_3^- deficits from the water column rather than NO_3^- turbulent diffusion as our proxy for NO_3^- assimilation (Fig. 2). The fluxes of NO_3^- assimilation calculated from the ΔNO_3^- were 2.1 and 4.6 mmol m^{-2} d^{-1} for December 2016 and February 2017, respectively, and the fluxes of N_2 fixation measured for these months was 0.03 and 0.08 mmol m^{-2} d^{-1}, respectively. Accordingly, NP was estimated (by Eqs. 1, 2) as 2.2 and 4.7 mmol m^{-2} d^{-1} for these months and the calculated fraction of N_2 fixation of total NP was estimated at 1–2%.

Estimating NP during transition (onset of stratification)

During a period of 63 d (15 March–17 May) a net nitrogen decrease of 35 mmol N m^{-2} was observed in the photic water column, which translates to an average NO$_3^-$ uptake rate of 0.55 mmol N m^{-2} d^{-1}. The fluxes of photic N$_2$ fixation during April and May 2016 were 0.12 and 0.23 mmol N m^{-2} d^{-1}. Accordingly, the calculated fraction of N$_2$ fixation of total NP was estimated at 10% and 30% for April and May 2016, respectively. During April 2018, NO$_3^-$ uptake rates were considerably higher, 1.3 mmol N m^{-2} d^{-1}, while photic N$_2$ fixation was only 0.02 mmol N m^{-2} d^{-1}. Thus, the estimated contribution of N$_2$ fixation to NP decreased to less than 2%.

Estimating NP during stratification

Using Eq. 3 the fluxes of aphotic NO$_3$ $\left(F_{\text{aphotic NO}_3^-}\right)$ during July and September 2016 were estimated to be 0.22 and 0.11 mmol N m^{-2} d^{-1}, respectively, and 1.4 mmol N m^{-2} d^{-1} for July 2018. N$_2$ fixation fluxes (F_{NF}) in the photic zone were determined to be 0.08 mmol N m^{-2} d^{-1} for July and September, respectively, and 0.01 mmol N m^{-2} d^{-1} for July 2018. Utilizing the above, the calculated fraction of the photic N$_2$ fixation of NP during 2016 was 26% during July 2016, and 40% during September 2016, while during July 2018 this fraction was much lower making up less than 1% of the NP.

Estimating the *f* ratio during stratification

NP during the stratification period of 2016 was estimated at 0.18–0.3 mmol m^{-2} d^{-2}. PP rates (converted to N) were 1.2–1.5 mmol N m^{-2} d^{-2}. Accordingly, the *f* ratio during stratification was estimated at 0.1–0.2.

Discussion

Characterization and dynamics of diazotrophic communities of the Gulf

The outstanding feature obtained throughout our sampling was the preponderance of amplicons annotated to NCD, mostly from α- and γ-proteobacteria, and the almost complete lack of cyanobacterial diazotrophs—including the conspicuous *Trichodesmium* which is found in the Gulf on many occasions (Fig. 6). Our observations of the majority of amplicons retrieved from the photic water column affiliated with NCD, corresponded to a previous *nifH* survey (Foster et al. 2009), where 47 out of 73 sequences (clone libraries) were also affiliated with members of the α- and γ-proteobacteria. Global surveys of *nifH* (Farnelid et al. 2011; Delmont et al. 2022) and large datasets of specific *nifH* labeled images (Karlusich et al. 2021) also report that NCD prevail in oceanic photic zones, thus implying that that NCD are more abundant and widespread than their cyanobacterial counterparts throughout most of the global ocean's surface water. Moreover, the abundance of NCDs coupled with low rates of N$_2$ fixation as reported by others (Halm et al. 2012; Ridame et al. 2022) also corresponds with our findings of abundant NCDs in the photic layer of the Gulf linked to low rates of N$_2$ fixation.

ASV89, closely related to *M. purpuratum* and *P. stutzeri* (97% amino acid sequence identity of partial *nifH* sequences) was the most abundant amplicon throughout our samples when considering both photic and aphotic water (found in four of the eight samples from photic depths and seven of eight samples form aphotic depths; Fig. S7). This ASV comprised 80–95% of the reads retrieved from aphotic water (when maximal rates were mesured during mixing and re-stratification; April–May 2016; February 2017), but also comprised > 80% of the retrieved reads when measured rates were near detection limits (July 2016) (Figs. 4, S7; Table S2). *P. stutzeri* isolates were reported to fix N$_2$ under high oxygen concentrations (Bentzon-Tilia et al. 2015; Paerl et al. 2018), and sequences affiliated with this phylotype were recovered from samples collected from aphotic oxygenated water of the Levantine Basin when detectable N$_2$ fixation were measured (Rahav et al. 2013). The ability to fix N$_2$ under such conditions could be advantageous in the oxygenated water column of the Gulf, yet the specific conditions that trigger N$_2$ fixation in *P. stutzeri* are currently unknown.

Only three cyanobacterial amplicons were identified in our samples from the photic water and were recovered, from which two (ASVs 52–53) were clustered with *Candidatus Atelocyanobacterium thalassa* (UCYN-A) (Fig. S8). These amplicons shared 99–100% identity to sequences previously collected in the Gulf surface water during late stratification by Foster et al. (2009) which also reported these phylotypes to be "detected but not quantifiable" by qPCR. These sequences also shared > 98% identity to several UCYN-A isolates from the Pacific Ocean (Fig. S8). The extremely low abundance of these amplicons in our samples (< 2%), and with no direct evidence of cell-specific activity, prevent linking between the presence of these UCYN-A-like sequences although maximal high N$_2$ fixation rates measured at the time of their collection.

Surprisingly, we were unable to retrieve amplicons affiliated with *Trichodesmium* from any of our samples throughout the study period. *Trichodesmium* is frequently observed in surface water of the Gulf and was reported to appear during late stratification and early fall (Post et al. 2002; Foster et al. 2009; Wang et al. 2022), as well as after winter mixing (Rahav et al. 2013; Basu et al. 2019). Two of our sampling cruises (19 April and 5 May 2016) were carried within a time frame of 3 weeks when visible surface slicks of *Trichodesmium* were reported in the Gulf surface water (Gledhill et al. 2019) including the morning of our cruise on 5 May (Fig. S9), although visible slicks were not observed in St. A at the time of sampling. Reported *Trichodesmum* colony densities in the water column ranged from 1 to 100 colonies m^{-3} and increased to 10^6 colonies m^{-3} during bloom events (Post 2002), but visible slicks can also rapidly (< 30 min) dissipate (Gledhill et al. 2019). Considering the stochastic nature of *Trichodesmium*'s appearance in the Gulf water column (Post 2002), and our sampling resolution, we may have missed *Trichodesmium*. Maximal N$_2$ fixation rates were previously reported when *Trichodesmium* appeared (Foster

et al. 2009; Rahav et al. 2013). Thus, while our estimates of N_2 fixation rates may underestimate the actual annual budgets of N_2 fixation in Gulf, to our knowledge there are no large-scale blooms of *Trichodesmium* in the Gulf which would contribute considerably to the annual budget.

What does our data indicate regarding the contribution of the diverse diazotroph groups to water column N_2 fixation and PP? Amplicon abundance of different phylotypes may not necessarily reflect the relative contribution of each group to the water column's N_2-fixation, as measured by ^{15}N uptake of the bulk diazotroph community (Yogev et al. 2011; Turk-Kubo et al. 2014). Amplicon sequencing provides only relative abundances, which may be different from of the actual abundances of the target microorganism in the natural environment (Bonnet et al. 2021). Furthermore, previous studies suggest that rare phylotypes could disproportionately contribute to nitrogenase transcriptional activities, while other species can be more abundant, but less active (Turk-Kubo et al. 2014; Yang et al. 2019). Uncertainties such as bias of degenerated primers used for amplification (Gaby and Buckley 2012) and data of multiple genomes or *nifH* copies per cell possessed by some cyanobacterial diazotrophs (Foster and O'Mullan 2008; Sargent et al. 2016) is missing for NCD. Some NCD can exhibit unconventional regulation of N_2 fixation (Bombar et al. 2016). Direct field measurements or reported rates of N_2 fixation per cell are currently lacking for marine NCDs and the conditions that control N_2 fixation in NCD are not well constrained (Gradoville et al. 2017; Moisander et al. 2017). Twenty percent of the genomes from a large recent dataset of *nifH*-harboring phylotypes lacked the *nifD* and *nifK* genes (Mise et al. 2021). These organisms were considered incapable of active N_2 fixation despite harboring *nifH* and thus the presence of *nifH* does not necessarily portend a direct link to N_2 fixation.

In summary, the identities of specific diazotrophs responsible for N_2 fixation in the Gulf remain elusive. To better understand which diazotrophs are responsible for the observed N_2 fixation rates in the Gulf, coupling between specific identification and quantification of cell-specific rates of N_2 fixation is necessary, considering all uncertainties mentioned above.

N_2 fixation rates (Fig. 4; Table 1) and diazotroph community structure fluctuated in both photic and aphotic layers with no pronounced seasonal or interannual variations. Generally, our volumetric rates (above detection) are consistent with the lower end of reported volumetric rates from photic zones across global oceans (Luo et al. 2012; Tang et al. 2019) and are similar overall to those previously reported rates for the Gulf (Foster et al. 2009; Rahav et al. 2013).

The volumetric rates measured in aphotic depths were mostly < 0.5 nmol N L^{-1} d^{-1}, at the range of previous reports from the Gulf (0.06–0.58; Rahav et al. 2013), the Mediterranean Sea (Benavides et al. 2018), and the Pacific Ocean (Bonnet et al. 2013).

It is pertinent to note that the $^{15}N_2$ atom% in incubation bottles at the beginning of the experiments was calculated from the $^{15}N_2$ atom% of the "spike" of ESW stock, which could underestimate the actual $^{15}N_2$ atom% in incubation bottles (considering our ESW preparation method; *see* White et al. 2020—table 4). This calculation methodology was used, as the field and laboratory work were conducted prior to the study of White et al. (2020), which recommends measuring the isotopic composition of dissolved N_2 in each of spiked incubation bottles, rather than extrapolating $^{15}N_2$ atom% from that of the $^{15}N_2$-enriched inoculum.

How would winter vertical mixing and observed maximal MLD affect the observed rates? Both field and model studies suggested that diverse NCDs are present and thrive in sinking particles (Pedersen et al. 2018; Farnelid et al. 2019; Chakraborty et al. 2021) and in the export flux (Bonnet et al. 2023). Thus, the higher rates observed in aphotic water during deep mixing (February 2016; February–March 2017) could result from enhanced export fluxes of POM corresponding to winter mixing depth (Torfstein et al. 2020). This could explain the observed low (mostly below detection) rates measured in the samples collected in aphotic water during the stratified period (July–September 2016) when less particles are available for colonization in aphotic water due to extensive re-mineralization. This could also explain why most rates during 2018 (in both photic and aphotic depths) were below detection, following the shallow winter mixing.

The contribution of N_2 fixation to primary and NP

Photic zone N_2 fixation rates comprised 0.5–5% of the PP during the stratified period when PP was low and was typically lower during winter mixing and transition when PP is high (Table 2). An exception was May 2016, when maximal N_2 fixation rates were measured, and the contribution of photic N_2 fixation to PP increased to 12%. A more relevant estimate is, however, the contribution of N_2 fixation to NP. In typical oceanic environments, NP, especially during stratification, is considerably lower than PP (Yool et al. 2007) and hence, the contribution of N_2 fixation to PP is potentially high. In subtropical areas of the Pacific Ocean (global "hotspots" of N_2 fixation where *Trichodesmium* flourishes) the estimated contribution of N_2 fixation to NP under stratified conditions was higher than NO_3^- based NP and accounted for up to 90% in the Western Tropical South Pacific (Caffin et al. 2018). Studies from the Atlantic Ocean reported lower values, with N_2 fixation contributing to NP in the range of 2–41% (Mourino-Carballido 2011; Benavides et al. 2013; Moreira-Coello et al. 2017).

The contribution of photic N_2 fixation to NP

Atmospheric deposition, riverine input, and nutrient upwelling are considered as the major N sources for NP in addition to N_2 fixation (Platt et al. 1989). In the deserts surrounding the Gulf, no significant riverine inputs (excluding flash-floods) contribute to NP (Chen et al. 2007). Atmospheric deposition (i.e., dust) was suggested as a potential source of

Table 2. Estimated contribution of N_2 fixation to primary and new production. The contribution of photic N_2 fixation to primary productivity was estimated from the simultaneous measurements of N_2 fixation and primary productivity (^{15}N and ^{13}C uptake rates, respectively). The contribution to new production (NP) was estimated from N_2 fixation (^{15}N-uptake rates) and estimated new production ($NO_3^- + N_2$ fixation).

Cruise #	Sampling date	Water column stability	Estimated contribution to primary production	Estimated contribution to new production	
			Photic N_2 fixation	Photic N_2 fixation	Aphotic N_2 fixation
1	Feb 2016	Deep mixing	<1%	<1%	<1%
2	Apr 2016	Thermostabilizing	1%	10%	<1%
3	May 2016	Thermostabilizing	12%	30%	<1%
4	July 2016	Fully stratified	7%	26%	<1%
5	Sep 2016	Fully stratified	5%	40%	<1%
6	Dec 2016	Shallow mixing	1%	1%	<1%
7	Feb 2017	Deep mixing	1%	2%	2%
8	Mar 2017	Deep mixing	<1%	<1%	1%
9	Apr 2018	Thermostabilizing	9%	2%	<1%
10	Jul 2018	Fully stratified	<1%	1%	<1%
11	Dec 2018	Shallow mixing	2%	<1%	<1%

nitrogen supporting primary production in the Gulf (Wankel et al. 2010). Yet, more recently, dust did not appear to impact subsequent surface Chl *a* variations (Torfstein and Kienast 2018). Hence, here we defined NP in the Gulf as the sum of nitrogen fluxes from entrainment of deep water (aphotic) NO_3^- (either by vertical mixing during winter or by cross-thermocline turbulent mixing during summer) and from N_2 fixation.

Our calculations indicated that contributions of photic N_2 fixation to NP varied both seasonally and interannually. During the winter mixing our results clearly demonstrate that the main source of N for NP is nitrate that is transported to the upper surface layers and the contribution of the photic N_2 fixation to NP during the winter mixing rarely exceeded 1% (Table 2).

As the temperatures warm, the transition to a stratified water column alters the transport and availability of nutrients. During this period (transition from mixed to stratified water column) estimating the contribution of photic N_2 fixation to NP is challenging as the rapid shoaling of the MLD from its maximum depth to about 25 m complicates the estimates of vertical NO3- transport. Here we estimated the NO_3^- part of NP (the $F_{\text{aphotic NO}_3^-}$ member in Eq. 1) as the difference between the inventory of NO_3^- "trapped" in the photic zone at the beginning of thermal stratification and the small NO_3^- inventory in the photic zone when stratification had stabilized. Dividing this difference by the time interval between these two events, provided the NP fraction stemming from phytoplankton nutrient utilization and growth. Accordingly, we estimated N_2 fixation comprised 10–25% of NP during the transition period of 2016 (Table 2). This contribution is likely

the result of maximal N_2 fixation rates coinciding with reports of *Trichodesmium* slicks on surface water of the Gulf (Gledhill et al. 2019). The estimated contribution of N_2 fixation to NP during the thermostabilizing period of 2018 (no available reports of *Trichodesmium* abundance) was <2% (Table 2). When the water column is fully stratified (summer–fall), the contribution of N_2 fixation to NP increased (Table 2) with photic N_2 fixation making up ∼30% of the NP during the summer stratification of 2016 but <1% during the same period in 2018 (Table 2).

The NP and PP data utilized for estimating the *f* ratio (the fraction of NP from total primary production; Eppley and Peterson 1979) highlight the low contribution of NP during the summer stratification period of 2016 (*f* ratio: 0.05–0.1) emphasizing the predominance of regenerated production during the stratified period in the Gulf. To the best of our knowledge, this is the first estimate of the *f* ratio for the Gulf based on data from direct field measurements which include N_2 fixation. The previous estimate of the *f* ratio for the Gulf was based on a simple diffusivity model of NO_3^- fluxes calculated across a 50–150 m water column between May and November (early stratification to early mixing) (Badran et al. 2005). These NO_3^- samples were collected between 1995 and 2000 and compared with average PP rates reported by Levanon-Spanier et al. (1979). Here, we focus our estimates exclusively on data collected during the stratified period (June–September) and compare it with same-day PP measurements. Our estimation of NO_3^- fluxes during stratification (0.1–0.2 mmol m^{-2} d^{-1}) was 10–20-fold lower compared with Badran et al. (2005) and resulted with a 5–10-fold lower *f* ratio (0.05–0.1 vs. 0.5, reported by Badran et al. 2005).

The contribution of aphotic N_2 fixation to NP

Considering the large volume of aphotic waters in open ocean environments, the depth integrated rates of N_2 fixation in aphotic water could potentially be high, even if the rate per given water volume is low (Benavides et al. 2018). Yet, the contribution of aphotic N_2 fixation to NP is estimated to be rather small (last column in Table 2) because, by definition, NP is the PP term which is supported by nutrient inputs external to the photic zone. To estimate the contribution of aphotic N_2 fixation to NP we must determine when and how the remineralization products of the POM produced by aphotic N_2 fixation reach the photic zone as remineralized nitrogen. We assume that the POM originating from aphotic N_2 fixation during transition and stratification periods (April–October) remains at or below the thermocline (or even sinks to the sediment/water interface) until the MLD of the following mixing season (October–March) exceeds the depth of the photic zone (~ 100 m). During the mixing period, the remineralized N reaches the photic zone and is assimilated by the phytoplankton community. Based on these assumptions we estimate the maximum impact of this potential "new" nitrogen source to be very small, only ~ 1–2% of the average NO_3^- flux supplied to the photic zone by mixing of nutrient-replete deep water.

In summary, our estimates of the contribution of photic and aphotic N_2 fixation to NP (Table 2) demonstrate that photic zone N_2 fixation could be an important source of NP during summer stratification, when very limited NO_3^- and remineralization products of aphotic N_2 fixation are supplied from depth, by turbulent diffusion, across the thermocline. In winter, the contribution of N_2 fixation to NP during deep mixing is minor, despite the relatively higher aphotic N_2 fixation rates and the enhanced vertical transport to the surface during winter. The active vertical mixing during winter supplies considerably more NO_3^- to the photic layer than the combined N_2 fixation from photic and aphotic depths. We suggest that during warm winters, which are characterized by a shallow mixed layer, the contribution of N_2 fixation to NP will be greater. It is expected that the frequency of such warm winters will increase in the future with the impacts of global warming.

Significance of field observations for future biogeochemical models

Although N_2 fixation by NCDs and aphotic N_2 fixation may potentially contribute to global budgets (Moisander et al. 2017; Benavides et al. 2018; Zehr and Capone 2020), the limited understanding of the factors controlling NCD growth and activity hamper the attempt to quantify these sources, their contribution to PP and NP, and their subsequent application to biogeochemical models (Moore et al. 2004; Bombar et al. 2016).

Attempting this for the Gulf, Kuhn et al. (2018) developed a model that investigated the effects of photic and aphotic N_2 fixation by NCD (i.e., "heterotrophic" in publications), colonial and unicellular cyanobacterial diazotrophs on nutrient ratios (e.g., N/P) and PP in the the Gulf. Model simulations were run for the years 2006–2010 and compared with field data collected from the same years (including PP and N_2 fixation). The model results show that, for these years, the presence of heterotrophic, colonial, and unicellular cyanobacterial diazotrophs was required to simulate the vertical structure of nutrient ratios in the Gulf (Kuhn et al. 2018). Model versions which excluded one or more of these groups could not replicate field observations to the same level of success, suggesting all three diazotroph groups are important. The model, however, estimated that N_2 fixation makes up 10–14% of the total annual PP, in contrast to our assessment for the years 2016–2018, which was lower by a factor of 2–10 (1–5%). These discrepancies could reflect interannual variations, low vertical and temporal measurement resolution and incomplete model parametrization. Our measurements and observations here could be used to further examine model competence, constrain model parametrization, and improve simulation strategy of future versions of physical–biological models for the oceanic water column.

Finally, our study reveals a predominant NCD community and typically low N_2 fixation rates in both the photic and aphotic zone of the northern Gulf. The overall contribution of diazotrophy to PP and NP during spring–summer stratification in the Gulf accounted for 1–5% of the photic zone PP and ~ 3–30% of NP. During fall and winter the contribution of N_2 fixation declined to < 1% of the NP. We conclude that on an annual average, diazotrophy plays a minor role in the NP of the Gulf. Stochastic occurrences of small blooms of *Trichodesmium* or other cyanobacterial diazotrophs, as well as particle-associated diazotrophs may provide "hot spots" with temporally transient higher rates of fixation. Yet, the major "new" nitrogen sources are cross-thermocline turbulent diffusion of nitrate during summer stratification and vertical mixing of nitrate during the fall–winter

References

Al-Qutob, M., C. Häse, M. M. Tilzer, and B. Lazar. 2002. Phytoplankton drives nitrite dynamics in the Gulf of Aqaba, Red Sea. Mar. Ecol.: Prog. Ser. **239**: 233–239. doi:10.3354/meps239233

Badran, M. I., M. Rasheed, R. Manasrah, and T. Al-Najjar. 2005. Nutrient flux fuels the summer primary productivity in the oligotrophic waters of the Gulf of Aqaba, Red Sea. Oceanologia **47**: 47–60.

Basu, S., M. Gledhill, D. de Beer, S. P. Matondkar, and Y. Shaked. 2019. Colonies of marine cyanobacteria *Trichodesmium* interact with associated bacteria to acquire iron from dust. Commun. Biol. **2**: 284. doi:10.1038/s42003-019-0534-z

Benavides, M., J. Arístegui, N. S. Agawin, X. A. Álvarez-Salgado, M. Álvarez, and C. Troupin. 2013. Low contribution of N_2

fixation to new production and excess nitrogen in the subtropical Northeast Atlantic margin. Deep-Sea Res. I: Oceanogr. Res. Pap. **81**: 36–48. doi:10.1016/j.dsr.2013.07.004

Benavides, M., P. H. Moisander, H. Berthelot, T. Dittmar, O. Grosso, and S. Bonnet. 2015. Mesopelagic N_2 fixation related to organic matter composition in the Solomon and Bismarck seas (Southwest Pacific). PLoS One **10**: e0143775. doi:10.1371/journal.pone.0143775

Benavides, M., S. Bonnet, I. Berman-Frank, and L. Riemann. 2018. Deep into oceanic N_2 fixation. Front. Mar. Sci. **5**: 108. doi:10.3389/fmars.2018.00108

Benavides, M., and others. 2022. Sinking *Trichodesmium* fixes nitrogen in the dark ocean. ISME J. **16**: 2398–2405. doi:10.1038/s41396-022-01289-6

Bentzon-Tilia, M., S. J. Traving, M. Mantikci, H. Knudsen-Leerbeck, J. L. S. Hansen, S. Markager, and L. Riemann. 2015. Significant N_2 fixation by heterotrophs, photo-heterotrophs and heterocystous cyanobacteria in two temperate estuaries. ISME J. **9**: 273–285. doi:10.1038/ismej.2014.119

Biton, E., and H. Gildor. 2011. The coupling between exchange flux through a strait and dynamics in a small convectively driven marginal sea: The Gulf of Aqaba (Gulf of Eilat). J. Geophys. Res.: Oceans **116**: C06017. doi:10.1029/2010JC00686010.1029/2011JC007106

Bolyen, E., and others. 2019. Reproducible, interactive, scalable and extensible microbiome data science using QIIME 2. Nat. Biotechnol. **37**: 852–857. doi:10.1038/s41587-019-0209-9

Bombar, D., R. W. Paerl, and L. Riemann. 2016. Marine non-cyanobacterial diazotrophs: Moving beyond molecular detection. Trends Microbiol. **24**: 916–927. doi:10.1016/j.tim.2016.07.002

Bonnet, S., Benavides, M., Le Moigne, F. A. C., Camps, M., Torremocha, A., Grosso, O., Dimier, C., Spungin, D., Berman-Frank, I., Garczarek, L., & Cornejo-Castillo, F. M. 2021. *Massive export of diazotrophs across the South Pacific tropical Ocean*. https://doi.org/10.1101/2021.05.07.442706

Bonnet, S., J. Dekaezemacker, K. A. Turk-Kubo, T. Moutin, R. M. Hamersley, O. Grosso, J. P. Zehr, and D. G. Capone. 2013. Aphotic N_2 fixation in the eastern tropical South Pacific Ocean. PLoS One **8**: e81265. doi:10.1371/journal.pone.0081265

Bonnet, S., and others. 2023. Diazotrophs are overlooked contributors to carbon and nitrogen export to the deep ocean. ISME J. **17**: 47–58. doi:10.1038/s41396-022-01319-3

Caffin, M., T. Moutin, and others. 2018. N_2 fixation as a dominant new N source in the western tropical South Pacific Ocean (OUTPACE cruise). Biogeosciences **15**: 2565–2585. doi:10.5194/bg-15-2565-2018

Capone, D. G., and E. J. Carpenter. 1982. Nitrogen fixation in the marine environment. Science **217**: 1140–1142. doi:10.1126/science.217.4565.1140

Capone, D. G., J. A. Burns, J. P. Montoya, A. Subramaniam, C. Mahaffey, T. Gunderson, A. F. Michaels, and E. J. Carpenter. 2005. Nitrogen fixation by *Trichodesmium* spp.: An important source of new nitrogen to the tropical and subtropical North Atlantic Ocean. Glob. Biogeochem. Cycles **19**: 1–17. doi:10.1029/2004GB002331

Carlson, D. F., E. Fredj, and H. Gildor. 2014. The annual cycle of vertical mixing and restratification in the northern Gulf of Eilat/Aqaba (Red Sea) based on high temporal and vertical resolution observations. Deep-Sea Res. I: Oceanogr. Res. Pap. **84**: 1–17. doi:10.1016/j.dsr.2013.10.004

Chakraborty, S., K. H. Andersen, A. W. Visser, K. Inomura, M. J. Follows, and L. Riemann. 2021. Quantifying nitrogen fixation by heterotrophic bacteria in sinking marine particles. Nat. Commun. **12**: 4085. doi:10.1038/s41467-021-23875-6

Chen, Y., S. Mills, J. Street, D. Golan, A. Post, M. Jacobson, and A. Paytan. 2007. Estimates of atmospheric dry deposition and associated input of nutrients to Gulf of Aqaba seawater. J. Geophys. Res.: Atmospheres **112**: 1–14. doi:10.1029/2006JD007858

Chien, Y. T., and S. H. Zinder. 1996. Cloning, functional organization, transcript studies, and phylogenetic analysis of the complete nitrogenase structural genes (*nifHDK2*) and associated genes in the archaeon *Methanosarcina barkeri* 227. J. Bacteriol. **178**: 143–148. doi:10.1128/jb.178.1.143-148.1996

David, E. 2002. Vertical distribution and fluxes of dissolved inorganic nitrogen and phytoplankton in the northern Gulf of Aqaba (Elat). M.Sc. thesis. HUJI.

Delmont, T. O., and others. 2022. Heterotrophic bacterial diazotrophs are more abundant than their cyanobacterial counterparts in metagenomes covering most of the sunlit ocean. ISME J. **16**: 927–936. doi:10.1038/s41396-021-01135-1

Dugdale, R., and J. Goering. 1967. Uptake of new and regenerated forms of nitrogen in primary productivity. Limnol. Oceanogr. **12**: 196–206. doi:10.4319/lo.1967.12.2.0196

Eppley, R. W., and B. J. Peterson. 1979. Particulate organic matter flux and planktonic new production in the deep ocean. Nature **282**: 677–680. doi:10.1038/282677a0

Farnelid, H., and others. 2011. Nitrogenase gene amplicons from global marine surface waters are dominated by genes of non-cyanobacteria. PLoS One **6**: e19223. doi:10.1371/journal.pone.0019223

Farnelid, H., K. Turk-Kubo, H. Ploug, J. E. Ossolinski, J. R. Collins, B. A. van Mooy, and J. P. Zehr. 2019. Diverse diazotrophs are present on sinking particles in the North Pacific subtropical gyre. ISME J. **13**: 170–182. doi:10.1038/s41396-018-0259-x

Foster, R. A., and G. D. O'Mullan. 2008. Nitrogen-fixing and nitrifying symbioses in the marine environment, p. 1197–1218. *In* D. G. Capone, D. A. Bronk, M. R. Mulholland, and

E. J. Carpenter [eds.], Nitrogen in the marine environment. Academic Press.

Foster, R., A. Paytan, and J. Zehr. 2009. Seasonality of N$_2$ fixation and *nifH* gene diversity in the Gulf of Aqaba (Red Sea). Limnol. Oceanogr. **54**: 219–233. doi:10.4319/lo.2009.54.1.0219

Frank, I. E., K. A. Turk-Kubo, and J. P. Zehr. 2016. Rapid annotation of *nifH* gene sequences using classification and regression trees facilitates environmental functional gene analysis. Environ. Microbiol. Rep. **8**: 905–916. doi:10.1111/1758-2229.12455

Gaby, J. C., and D. H. Buckley. 2012. A comprehensive evaluation of PCR primers to amplify the *nifH* gene of nitrogenase. PloS One **9**: e93883. doi:10.1371/journal.pone.0042149

Genin, A., B. Lazar, and S. Brenner. 1995. Vertical mixing and coral death in the Red Sea following the eruption of Mount Pinatubo. Nature **377**: 507–510. doi:10.1038/377507a0

Gledhill, M., S. Basu, and Y. Shaked. 2019. Metallophores associated with *Trichodesmium erythraeum* colonies from the Gulf of Aqaba. Metallomics **11**: 1547–1557. doi:10.1039/C9MT00121B

Gradoville, M. R., D. Bombar, B. C. Crump, R. M. Letelier, J. P. Zehr, and A. E. White. 2017. Diversity and activity of nitrogen-fixing communities across ocean basins. Limnol. Oceanogr. **62**: 1895–1909. doi:10.1002/lno.10542

Großkopf, T., and others. 2012. Doubling of marine dinitrogen-fixation rates based on direct measurements. Nature **488**: 361–364. doi:10.1038/nature11338

Halm, H., and others. 2012. Heterotrophic organisms dominate nitrogen fixation in the South Pacific Gyre. ISME J. **6**: 1238–1249. doi:10.1038/ismej.2011.182

Hamme, R. C., and S. R. Emerson. 2004. The solubility of neon, nitrogen and argon in distilled water and seawater. Deep-Sea Res. I: Oceanogr. Res. Pap. **51**: 1517–1528. doi:10.1016/j.dsr.2004.06.009

Harding, K., K. A. Turk-Kubo, R. E. Sipler, M. M. Mills, D. A. Bronk, and J. P. Zehr. 2018. Symbiotic unicellular cyanobacteria fix nitrogen in the Arctic Ocean. Proc. Natl. Acad. Sci. USA **115**: 13371–13375. doi:10.1073/pnas.1813658115

Holm-Hansen, O., C. J. Lorenzen, R. W. Holmes, and J. D. Strickland. 1965. Fluorometric determination of chlorophyll. ICES J. Mar. Sci. **30**: 3–15. doi:10.1093/icesjms/30.1.3

Karlusich, J. J. P., and others. 2021. Global distribution patterns of marine nitrogen-fixers by imaging and molecular methods. Nat. Commun. **12**: 4160. doi:10.1038/s41467-021-24299-y

Kimor, B., and B. Golandsky. 1977. Microplankton of the Gulf of Elat: Aspects of seasonal and bathymetric distribution. Mar. Biol. **42**: 55–67. doi:10.1007/BF00392014

Kuhn, A. M., K. Fennel, and I. Berman-Frank. 2018. Modelling the biogeochemical effects of heterotrophic and autotrophic N$_2$ fixation in the Gulf of Aqaba (Israel), Red Sea. Biogeosciences **15**: 7379–7401. doi:10.5194/bg-15-7379-2018

Langlois, R., T. Großkopf, M. Mills, S. Takeda, and J. LaRoche. 2015. Widespread distribution and expression of gamma a (UMB), an uncultured, diazotrophic, γ-proteobacterial *nifH* phylotype. PloS One **10**: e0128912. doi:10.1371/journal.pone.0128912

Lazar, B., J. Erez, J. Silverman, T. Rivlin, A. Rivlin, M. Dray, E. Meeder, and D. Iluz. 2008. Recent environmental changes in the chemical-biological oceanography of the Gulf of Aqaba (Eilat), p. 49–62. *In* F. D. Por [ed.], Aqaba-Eilat, the improbable gulf. Environment, biodiversity, and preservation. Magnes Press.

Letunic, I., and P. Bork. 2021. Interactive Tree Of Life (iTOL) v5: An online tool for phylogenetic tree display and annotation. Nucleic Acids Res. **49**: 293–296. doi:10.1093/nar/gkab301

Levanon-Spanier, I., E. Padan, and Z. Reiss. 1979. Primary production in a desert-enclosed sea—The Gulf of Elat (Aqaba), Red Sea. Deep-Sea Res. A: Oceanogr. Res. Pap. **26**: 673–685. doi:10.1016/0198-0149(79)90040-2

Lindell, D., and A. F. Post. 1995. Ultraphytoplankton succession is triggered by deep winter mixing in the Gulf of Aqaba (Eilat), Red Sea. Limnol. Oceanogr. **40**: 1130–1141. doi:10.4319/lo.1995.40.6.1130

Luo, Y.-W., and others. 2012. Database of diazotrophs in global ocean: Abundance, biomass and nitrogen fixation rates. Earth Syst. Sci. Data **4**: 47–73. doi:10.5194/essd-4-47-2012

Mackey, K. R., T. Rivlin, A. R. Grossman, A. F. Post, and A. Paytan. 2009. Picophytoplankton responses to changing nutrient and light regimes during a bloom. Mar. Biol. **156**: 1531–1546. doi:10.1007/s00227-009-1185-2

Man-Aharonovich, D., N. Kress, E. B. Zeev, I. Berman-Frank, and O. Béjà. 2007. Molecular ecology of *nifH* genes and transcripts in the eastern Mediterranean Sea. Environ. Microbiol. **9**: 2354–2363. doi:10.1111/j.1462-2920.2007.01353.x

Meeder, E. 2012. Dynamics of nitrogen species in the oceanic water column, the Gulf of Aqaba "natural experiment". Doctoral dissertation. Hebrew Univ. Jerusalem (HUJI).

Mise, K., Y. Masuda, K. Senoo, and H. Itoh. 2021. Undervalued pseudo-*nifH* sequences in public databases distort metagenomic insights into biological nitrogen fixers. mSphere **6**: e0078521. doi:10.1128/msphere.00785-21

Mohr, W., T. Grosskopf, D. W. Wallace, and J. LaRoche. 2010. Methodological underestimation of oceanic nitrogen fixation rates. PLoS One **5**: e12583. doi:10.1371/journal.pone.0012583

Moisander, P. H., R. A. Beinart, M. Voss, and J. P. Zehr. 2008. Diversity and abundance of diazotrophic microorganisms in the South China Sea during intermonsoon. ISME J. **2**: 954–967. doi:10.1038/ismej.2008.51

Moisander, P. H., M. Benavides, S. Bonnet, I. Berman-Frank, A. E. White, and L. Riemann. 2017. Chasing after non-cyanobacterial nitrogen fixation in marine pelagic environments. Front. Microbiol. **8**: 1736. doi:10.3389/fmicb.2017.01736

Montoya, J. P., M. Voss, P. Kahler, and D. G. Capone. 1996. A simple, high-precision, high-sensitivity tracer assay for N_2 fixation. Appl. Environ. Microbiol. **62**: 986–993. doi:10.1128/aem.62.3.986-993.1996

Moore, J. K., S. C. Doney, and K. Lindsay. 2004. Upper ocean ecosystem dynamics and iron cycling in a global three-dimensional model. Glob. Biogeochem. Cycles **18**: 1–21. doi:10.1029/2004GB002220

Moreira-Coello, V., B. Mouriño-Carballido, E. Marañón, A. Fernández-Carrera, A. Bode, and M. M. Varela. 2017. Biological N_2 fixation in the upwelling region off NW Iberia: Magnitude, relevance, and players. Front. Mar. Sci. **4**: 303. doi:10.3389/fmars.2017.00303

Mourino-Carballido, B., and others. 2011. Importance of N_2 fixation vs. nitrate eddy diffusion along a latitudinal transect in the Atlantic Ocean. Limnol. Oceanogr. **56**: 999–1007. doi:10.4319/lo.2011.56.3.0999

Mulholland, M. R., and P. W. Bernhardt. 2005. The effect of growth rate, phosphorus concentration, and temperature on N_2 fixation, carbon fixation, and nitrogen release in continuous cultures of *Trichodesmium* IMS101. Limnol. Oceanogr. **50**: 839–849. doi:10.4319/lo.2005.50.3.0839

Mulholland, M. R., and others. 2012. Rates of dinitrogen fixation and the abundance of diazotrophs in north American coastal waters between Cape Hatteras and Georges Bank. Limnol. Oceanogr. **57**: 1067–1083. doi:10.4319/lo.2012.57.4.1067

Paerl, R. W., T. N. Hansen, N. N. Henriksen, A. K. Olesen, and L. Riemann. 2018. N-fixation and related O_2 constraints on model marine diazotroph *Pseudomonas stutzeri* BAL361. Aquat. Microb. Ecol. **81**: 125–136. doi:10.3354/ame01867

Pedersen, J. N., D. Bombar, R. W. Paerl, and L. Riemann. 2018. Diazotrophs and N_2-fixation associated with particles in coastal estuarine waters. Front. Microbiol. **9**: 2759. doi:10.3389/fmicb.2018.02759

Platt, T., W. G. Harrison, M. R. Lewis, W. K. W. Li, S. Sathyendranath, R. E. Smith, and A. F. Vezina. 1989. Biological production of the oceans: The case for a consensus. Mar. Ecol.: Prog. Ser. **52**: 77–88. doi:10.3354/meps052077

Post, A., and others. 2002. Spatial and temporal distribution of *Trichodesmium* spp. in the stratified Gulf of Aqaba, Red Sea. Mar. Ecol.: Prog. Ser. **239**: 241–250. doi:10.3354/meps239241

Rahav, E., E. Bar-Zeev, S. Ohayon, H. Elifantz, N. Belkin, B. Herut, M. R. Mulholland, and I. Berman-Frank. 2013. Dinitrogen fixation in aphotic oxygenated marine environments. Front. Microbiol. **4**: 227. doi:10.3389/fmicb.2013.00227

Ridame, C., and others. 2022. N_2 fixation in the Mediterranean Sea related to the composition of the diazotrophic community and impact of dust under present and future environmental conditions. Biogeosciences **19**: 415–435. doi:10.5194/bg-19-415-2022

Saitou, N., and M. Nei. 1987. The neighbor-joining method: A new method for reconstructing phylogenetic trees. Mol. Biol. Evol. **4**: 406–425. doi:10.1093/oxfordjournals.molbev.a040454

Sargent, E. C., A. Hitchcock, S. A. Johansson, R. Langlois, C. M. Moore, J. LaRoche, A. J. Poulton, and T. S. Bibby. 2016. Evidence for polyploidy in the globally important diazotroph *Trichodesmium*. FEMS Microbiol. Lett. **363**: fnw244. doi:10.1093/femsle/fnw244

Shaked, Y., and A. Genin. 2021. Scientific report for 2020, Israel National Monitoring Program at the Gulf of Elat (Hebrew with English abstract). The Ministry of Environmental Protection.

Shiozaki, T., A. Fujiwara, K. Inomura, Y. Hirose, F. Hashihama, and N. Harada. 2020. Biological nitrogen fixation detected under Antarctic Sea ice. Nat. Geosci. **13**: 729–732. doi:10.1038/s41561-020-00651-7

Stecher, G., K. Tamura, and S. Kumar. 2020. Molecular evolutionary genetics analysis (MEGA), molecular evolutionary genetics analysis (MEGA) for macOS for macOS. Mol. Biol. Evol. **37**: 1237–1239. doi:10.1093/molbev/msz312

Suggett, D. J., and others. 2009. Nitrogen and phosphorus limitation of oceanic microbial growth during spring in the Gulf of Aqaba. Aquat. Microb. Ecol. **56**: 227–239. doi:10.3354/ame01357

Tang, W., Z. Li, and N. Cassar. 2019. Machine learning estimates of global marine nitrogen fixation. J. Geophys. Res.: Biogeosciences **124**: 717–730. doi:10.1029/2018JG004828

Torfstein, A., and S. Kienast. 2018. No correlation between atmospheric dust and surface ocean chlorophyll *a* in the oligotrophic Gulf of Aqaba, northern Red Sea. J. Geophys. Res.:Biogeosciences **123**: 391–405. doi:10.1002/2017JG004063

Torfstein, A., S. S. Kienast, B. Yarden, A. Rivlin, S. Isaacs, and Y. Shaked. 2020. Bulk and export production fluxes in the Gulf of Aqaba, northern Red Sea. ACS Earth Space Chem. **4**: 1461–1479. doi:10.1021/acsearthspacechem.0c00079

Turk-Kubo, K. A., M. Karamchandani, D. G. Capone, and J. P. Zehr. 2014. The paradox of marine heterotrophic nitrogen fixation: Abundances of heterotrophic diazotrophs do not account for nitrogen fixation rates in the eastern tropical South Pacific. Environ. Microbiol. **16**: 3095–3114. doi:10.1111/1462-2920.12346

Wang, S., C. Koedooder, F. Zhang, N. Kessler, M. Eichner, D. Shi, and Y. Shaked. 2022. Colonies of the marine cyanobacterium *Trichodesmium* optimize dust utilization by selective collection and retention of nutrient-rich particles. iScience **25**: 103587. doi:10.1016/j.isci.2021.103587

Wankel, S. D., Y. Chen, C. Kendall, A. F. Post, and A. Paytan. 2010. Sources of aerosol nitrate to the Gulf of Aqaba: Evidence from $\delta^{15}N$ and $\delta^{18}O$ of nitrate and trace metal

chemistry. Mar. Chem. **120**: 90–99. doi:10.1016/j.marchem.2009.01.013

White, A. E., and others. 2020. A critical review of the $^{15}N_2$ tracer method to measure diazotrophic production in pelagic ecosystems. Limnol. Oceanogr.: Methods **18**: 129–147. doi:10.1002/lom3.10353

Wilson, S. T., D. Böttjer, M. J. Church, and D. M. Karl. 2012. Comparative assessment of nitrogen fixation methodologies, conducted in the oligotrophic North Pacific Ocean. Appl. Environ. Microbiol. **78**: 6516–6523. doi:10.1128/AEM.01146-12

Wolf-Vecht, A., N. Paldor, and S. Brenner. 1992. Hydrographic indications of advection/convection effects in the Gulf of Eilat. Deep-Sea Res. A: Oceanogr. Res. Pap. **39**: 1393–1401. doi:10.1016/0198-0149(92)90075-5

Yang, Q.-S., and others. 2019. Analysis of *nifH* DNA and RNA reveals a disproportionate contribution to nitrogenase activities by rare plankton-associated diazotrophs. BMC Microbiol. **19**: 188. doi:10.1186/s12866-019-1565-9

Yogev, T., and others. 2011. Is dinitrogen fixation significant in the Levantine Basin, East Mediterranean Sea? Environ. Microbiol. **13**: 854–871. doi:10.1111/j.1462-2920.2010.02402.x

Yool, A., A. P. Martin, C. Fernández, and D. R. Clark. 2007. The significance of nitrification for oceanic new production. Nature **447**: 999–1002. doi:10.1038/nature05885

Zani, S., M. T. Mellon, J. L. Collier, and J. P. Zehr. 2000. Expression of *nifH* genes in natural microbial assemblages in Lake George, New York, detected by reverse transcriptase PCR. Appl. Environ. Microbiol. **66**: 3119–3124. doi:10.1128/aem.66.7.3119-3124.2000

Zehr, J. P., and L. A. McReynolds. 1989. Use of degenerate oligonucleotides for amplification of the *nifH* gene from the marine cyanobacterium *Trichodesmium thiebautii*. Appl. Environ. Microbiol. **55**: 2522–2526. doi:10.1128/aem.55.10.2522-2526.1989

Zehr, J. P., L. L. Crumbliss, M. J. Church, E. O. Omoregie, and B. D. Jenkins. 2003. Nitrogenase genes in PCR and RT-PCR reagents: Implications for studies of diversity of functional genes. Biotechniques **35**: 996–1005. doi:10.2144/03355st08

Zehr, J. P., and D. G. Capone. 2020. Changing perspectives in marine nitrogen fixation. Science **368**: eaay9514. doi:10.1126/science.aay9514

Acknowledgments

Conflict of Interest

None declared.